THE JOURNAL OF PHYSICAL CHEMISTRY B

Article

pubs.acs.org/JPCB

Free Energy Calculations of Crystalline Hard Sphere Complexes Using Density Functional Theory

K. G. S. H. Gunawardana[†] and Xueyu Song*[,†,‡]

[†]Ames Laboratory and [‡]Department of Chemistry, Iowa State University, Ames, Iowa 50011, United States

ABSTRACT: Recently developed fundamental measure density functional theory (FMT) is used to study binary hard sphere (HS) complexes in crystalline phases. By comparing the excess free energy, pressure, and phase diagram, we show that the fundamental measure functional yields good agreements to the available simulation results of AB, AB_2, and AB_{13} crystals. Furthermore, we use this functional to study the HS models of five binary crystals, $Cu_5Zr(C15_b)$, $Cu_{51}Zr_{14}(\beta)$, $Cu_{10}Zr_7(\phi)$, CuZr(B2), and $CuZr_2(C11_b)$, which are observed in the Cu−Zr system. The FMT functional gives a well-behaved minimum for most of the hard sphere crystal complexes in the two-dimensional Gaussian parameter space, namely a crystalline phase. However, the current version of FMT functional (White Bear) fails to give a stable minimum for the structure $Cu_{10}Zr_7(\phi)$. We argue that the observed solid phases for the HS models of the Cu−Zr system are true thermodynamic stable phases and can be used as a reference system in perturbation calculations.

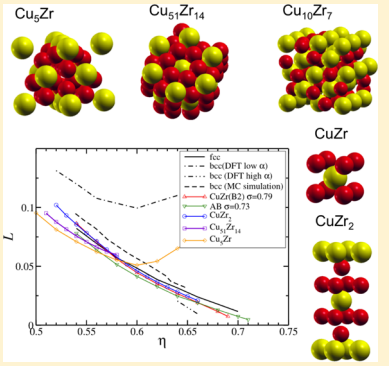

1. INTRODUCTION

As an alternative route of solving the many-body classical system efficiently the density functional theory (DFT) has been widely used recently.[1] One of the major strategies for practical applications to real systems, the perturbation approach, namely the system can be mapped to an effective hard sphere system and a perturbation part representing the attractive interactions, has been very successful.[2] In this case, the free energy of the hard sphere system can be calculated using the classical DFT, which has a universal functional form, plus a perturbation part from the detailed interactions of the system. This approach has been successfully applied to various systems including liquids,[2,3] simple solids,[4,5] and metallic systems.[6,7]

On the other hand, applications of this strategy to complex crystal structures are still rare due to unknown behaviors of the hard sphere functional. The recently developed fundamental measure theory (FMT) functional[8,9] has been found successful in describing thermodynamic properties of inhomogeneous hard sphere liquids,[10] crystals,[4,5] and interfaces.[3,11,12] However, the accuracy of this functional has not been studied for multicomponent hard sphere crystals to the best of our knowledge. In this paper, several complex binary hard sphere crystal structures observed in model systems and metallic systems are studied using the FMT functional.

The FMT is a result of the pioneered work of Rosenfeld,[8,9] who discovered that some geometrical measures of hard spheres can be related to the scaled particle theories through a set of weight functions. Later, the FMT functional was subjected to several refinements to improve its accuracy. Specially, the correction due to the dimensional analysis,[13] the addition of the tensor weight functions,[4] and the inclusion of the accurate empirical Mansoori−Carnahan−Starling−Leland (MCSL) equation of state instead of the approximate Percus−Yervick equation of state[3,11,14] are the major improvements of FMT. This latest version of FMT is known as the "White Bear" (WB) functional and is employed to study binary crystals in this work.

In this paper, we report that the FMT gives a well-behaved minimum for most binary systems in the two-dimensional Gaussian parameter space representing a solid phase. First, the following stable binary hard sphere crystals: AB_2, AB_{13}, and AB(CsCl) are studied as these structures have been studied previously by molecular simulations,[15−18] mean field theory,[19−21] and experiments.[22−25] We present detailed evidence that the FMT results yield good agreements with results from simulations and experiments by comparing excess free energy, equation of state, and phase stability. Moreover, for further practical applications of the FMT to more realistic systems, hard sphere models of the structures found in Cu−Zr systems are studied extensively, namely $Cu_5Zr(C15_b)$ prototype of Be_5Au, $Cu_{51}Zr_{14}(\beta)$,[26] $Cu_{10}Zr_7(\phi)$ prototype of $Ni_{10}Zr_7$,[27,28] CuZr(B2) prototype of CsCl,[29] and $CuZr_2(C11_b)$.[30] Analysis of the Lindemann ratio (L) of these binary crystals shows the existence of well-behaved solid phases in the two-dimensional Gaussian parameter space. The $CuZr_2$ and CuZr(B2) structures clearly show the vanishing of L as density reaching to the close packing limit, but L of the Cu_5Zr structure shows a similar behavior as a previously reported anomaly of the bcc lattice.[31] However, in lower packing fractions, the L is near the that of fcc and would potentially describe a solid phase. It was also found that out of all the seven different hard sphere model structures studied, only the $Cu_{10}Zr_7(\phi)$ structure did not show a

Special Issue: Branka M. Ladanyi Festschrift

Received: September 8, 2014
Revised: December 10, 2014

   dx.doi.org/10.1021/jp5090907 | J. Phys. Chem. B XXXX, XXX, XXX−XXX

minimum in the Gaussian parameter space; namely, it exists as a thermodynamically stable hard sphere crystal. In combination with the problems of other hard sphere lattices our work may also provide some pointers for the further improvement of the fundamental measure DFT.

This paper is organized as follows. In section 2, we summarize the basic ingredients of the "White Bear" functional of the fundamental measure theory used in our work. Then in section 3 the results of AB_2, AB_{13}, and AB stable hard sphere crystals are compared with simulations. In section 4 the hard sphere models of the above-mentioned crystals in the Cu−Zr system are presented to pave the way for another paper where the calculation of Cu−Zr phase diagram is presented. A detailed discussion on the observed failures of the latest WB FMT functional is provided in section 5. Finally, some concluding remarks are provided in section 6.

2. FUNDAMENTAL MEASURE THEORY

The density functional theory for many body classical systems follows the Mermin theorem.[1,32] Given the grand canonical ensemble, there exists a functional of single particle density distributions $\rho_i(\vec{r})$ such that

$$\Omega[\rho_1, \rho_2, ..., \rho_\nu] = F[\rho_1, \rho_2, ..., \rho_\nu] + \sum_{i=1}^{\nu} \int d^3r\, \rho_i(\vec{r})(V_i^{ext}(\vec{r}) - \mu_i) \tag{1}$$

where $V_i^{ext}(\vec{r})$ is the external potential and μ_i is the chemical potential of species i. The functional describing the Helmholtz free energy $F[\rho_1, \rho_2, ..., \rho_\nu]$ is independent of the external potential. The equilibrium density distributions $\rho_i^0(\vec{r})$ and the grand potential can be obtained by the variational principle

$$\left.\frac{\delta\Omega[\rho_1, \rho_2, ..., \rho_\nu]}{\delta\rho_i}\right|_{(\rho_i(\vec{r})=\rho_i^0(\vec{r}))} = 0 \tag{2}$$

When studying a crystalline phase, the density profile is assumed to be of a Gaussian form centered at each lattice site. The density profile of species i in a multicomponent system can be expressed as

$$\rho_i(\vec{r}) = \left(\frac{\alpha_i}{\pi}\right)^{3/2} \sum_{\vec{r}_i} e^{-\alpha_i(\vec{r}-\vec{r}_i)^2} \tag{3}$$

where α is the Gaussian parameter and $\vec{r}_i$ is the location of species i. The summation covers all the sites occupied by species i. The system is scaled with respect to the diameter of the largest species (d_A), and the diameter ratio is defined as $\sigma = d_B/d_A$. Then the minimization of the free energy functional is performed with respect to the dimensionless Gaussian parameters, $\alpha_i d_A^2$.

The Helmholtz free energy functional of a mixture of ν species can be split into two parts:

$$\beta F[\rho_1, \rho_2, ..., \rho_\nu] = \sum_{i=1}^{\nu} \int d^3\vec{r}(\ln(\rho_i(\vec{r})\Lambda_i^3) - 1)\rho_i(\vec{r}) + \beta F_{ex}[\rho_1, \rho_2, ..., \rho_\nu] \tag{4}$$

where Λ_i is the de Broglie wavelength of species i and $\beta = 1/k_BT$. The first part in the right-hand side of eq 4 gives the contribution due to the noninteracting particles and the later is the excess free energy.

In the fundamental measure theory, the hard sphere interaction contribution to the excess free energy functional can be expressed in terms of weighted densities as[8,9]

$$\beta F_{ex}[\{\rho_i\}] = \int d^3\vec{r}' \sum_{j=1}^{3} \Phi_j(\eta(\vec{r}), n_i(\vec{r}), \vec{v}_i(\vec{r}), \mathcal{T}_i(\vec{r})) \tag{5}$$

where the two scalar ($\eta_i(\vec{r})$ and $n_i(\vec{r})$), a vector ($v_i(\vec{r})$), and a tensor ($\mathcal{T}_i(\vec{r})$) weighted densities[3,11] are defined as the following:

$$\eta(\vec{r}) = \sum_{i=1}^{\nu} \int d^3\vec{r}'\, \rho_i(\vec{r}')\Theta(R_i - |\vec{r} - \vec{r}'|) \tag{6}$$

$$n_i(\vec{r}) = \frac{1}{4\pi R_i^2} \int d^3\vec{r}'\, \rho_i(\vec{r}')\delta(R_i - |\vec{r} - \vec{r}'|) \tag{7}$$

$$\vec{v}_i(\vec{r}) = \frac{1}{4\pi R_i^2} \int d^3\vec{r}'\, \rho_i(\vec{r}')\delta(R_i - |\vec{r} - \vec{r}'|)\frac{\vec{r} - \vec{r}'}{R_i} \tag{8}$$

$$\mathcal{T}_i^{m,n}(\vec{r}) = \frac{1}{4\pi R_i^2} \int d^3\vec{r}'\, \rho_i(\vec{r}')\delta(R_i - |\vec{r} - \vec{r}'|) \times \frac{(\vec{r} - \vec{r}')_m(\vec{r} - \vec{r}')_n}{R_i^2} \tag{9}$$

where $\mathcal{T}_i^{m,n}(\vec{r})$, $(m, n = 1, 2, 3)$, are the tensor components. The function $\Theta(x)$ is the Heaveside step function, and $\delta(x)$ is the Dirac delta function. The R_i is the hard sphere radius of species i. In the WB version of FMT the functional Φ_i are

$$\Phi_1[\rho] = -\int d^3\vec{r}\, \ln[1 - \eta(\vec{r})] \sum_{i=1}^{\nu} n_i(\vec{r}) \tag{10}$$

$$\Phi_2[\rho] = 2\pi \sum_{i,j=1}^{\nu} R_iR_j(R_i + R_j) \times \int d^3\vec{r} \frac{n_i(\vec{r})n_j(\vec{r}) - \vec{v}_i(\vec{r})\cdot\vec{v}_j(\vec{r})}{1 - \eta(\vec{r})} \tag{11}$$

and

$$\Phi_3[\rho] = 12\pi^2 \sum_{i,j,k=1}^{\nu} R_i^2R_j^2R_k^2 \int d^3\vec{r}\, \varphi_{ijk}(\vec{r})f_3(\eta(\vec{r})) \tag{12}$$

where

$$\varphi_{ijk}(\vec{r}) = \vec{v}_i\cdot\mathcal{T}_j\cdot\vec{v}_k - n_j\vec{v}_i\cdot\vec{v}_k - \mathrm{Tr}[\mathcal{T}_i\mathcal{T}_j\mathcal{T}_k] + n_j\mathrm{Tr}[\mathcal{T}_i\mathcal{T}_k] \tag{13}$$

and

$$f_3(\eta) = \frac{2}{3\eta}\left(\frac{\eta}{(1 - \eta)^2} + \ln(1 - \eta)\right) \tag{14}$$

In order to compare with the simulation results, the excess free energy is calculated by subtracting the ideal gas component in the liquid limit from the total free energy calculated from the FM-DFT. In the liquid limit, ideal gas component of a binary mixture can be expressed as, if $m_A/m_B = (d_A/d_B)^3$ is used,[19]

dx.doi.org/10.1021/jp5090907 | J. Phys. Chem. B XXXX, XXX, XXX−XXX

$$\frac{F_{id}}{N} = \left\{ \ln(\rho {d_A}^3) - 1 + \sum_{i=A,B} x_i \ln(x_i) + x_B \frac{9}{2} \ln(d_A/d_B) \right\} + \ln({\Lambda_A}^3/{d_A}^3) \quad (15)$$

where x_i (i = A, B) is the composition of species i in the compound and Λ_A is the de Broglie wavelength of the larger species. The dimensionless atomic number density is defined as $\rho {d_A}^3 = 6\eta/(\pi(x_A + x_B\sigma^3))$ where η is the packing fraction of the system and $\sigma = d_B/d_A$ is the diameter ratio of the hard spheres. The last term is left as the scaling of the system, and the excess free energy differs by the amount $\ln({\Lambda_A}^3/{d_A}^3)$.[15]

3. COMPARISON OF FMT RESULTS OF AB, AB_2, and AB_{13} WITH SIMULATIONS

The Helmholtz free energy for a given structure is obtained by minimizing the free energy functional, eq 4, with respect to the normalized Gaussian parameters as mentioned previously. This is a two-dimensional minimization for binary crystals. The normalized Gaussian parameters $\alpha_i {d_A}^2$ which give the minimum of eq 4 for each structure are plotted in Figure 1, where i = A, B

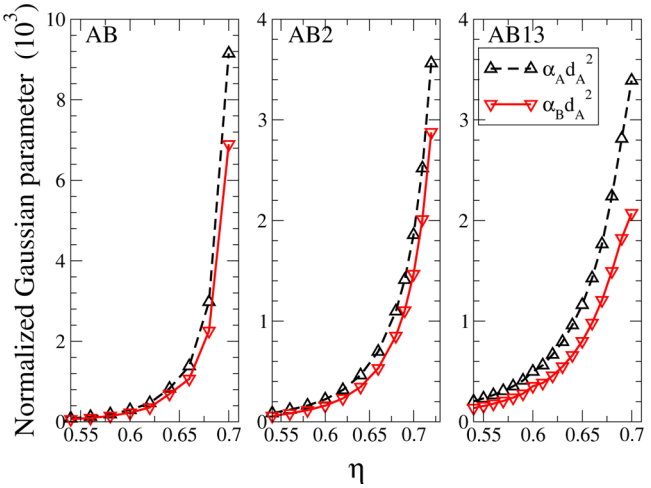

Figure 1. Normalized Gaussian parameter $\alpha_i {d_A}^2$ as a function of packing fraction η. The solid lines refer to the larger species i = A, and the dashed line refers to smaller species i = B.

refers to the species A and B. The smaller species (B) always have the smaller Gaussian parameter, implying their density is more smeared out to stabilize the structure despite of its smaller size. In these calculations the hard sphere diameter ratio of AB_2 and AB_{13} structures are at 0.58, and that of AB (CsCl) is at 0.73 as there exist detailed simulation results at these ratios and crystal structures.[15,16]

Figure 2 shows the excess free energy as a function of the packing fraction for AB, AB_2, and AB_{13} structures. Simulation results (dashed line) are extracted from Jackson et al.[18] For AB_{13} structure the calculated excess free energies are very close to simulation results at lower packing fractions. The percentage discrepancy is less that 1% at $\eta \approx 0.54$. However, the excess free energy of AB and AB_2 structures shows considerable discrepancy at lower η (about 7% at $\eta \approx 0.54$), and the discrepancy reduces as reaching to the higher η.

The pressure is calculated from the total Helmholtz free energy as

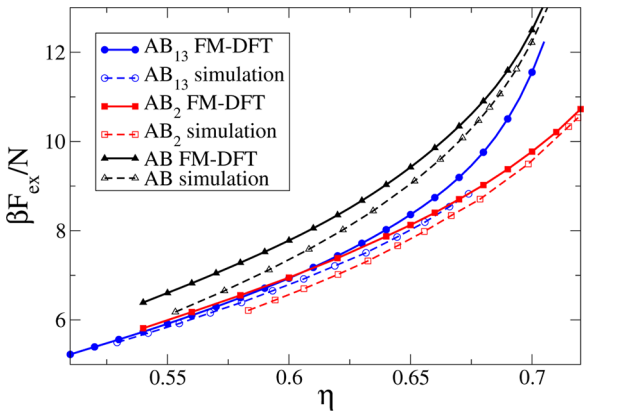

Figure 2. Excess free energy as a function of packing fraction η, for AB (up traingles), AB_2 (squares), and AB_{13} (circles) structures. The solid lines with symbols are calculated from the FMT in this work. The dashed lines with open symbols are the corresponding simulation results from ref 18.

$$P = \rho^2 \frac{\partial F/N}{\partial \rho} \quad (16)$$

In Figure 3 is plotted (solid lines) the dimensionless pressure $\beta P {d_A}^3$ as a function of η. The pressure shows an excellent

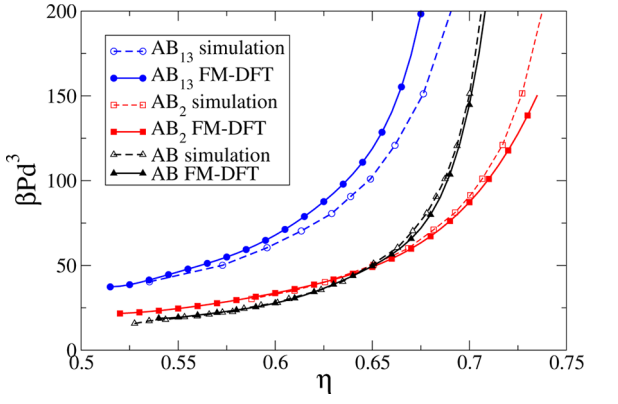

Figure 3. Pressure as a function of packing fracion η for AB (up traingles), AB_2 (squares), and AB_{13} (circles) structures. The parameter d_A is the diameter of the larger sphere. The solid lines with symbols are calculated from the FMT, and the dashed lines with open symbols are the corresponding simulation results from ref 18.

agreement with the simulation data of the AB and AB_2 structures. For AB_{13}, there is a noticeable deviation from the simulation at higher packing fractions. The corresponding simulation data (dashed lines) are also taken from ref 18.

However, what is important experimentally is the thermodynamic phase stability. To this end, the stability of these binary crystals with respect to the fluid phase of A and B[33] and fcc solid are studied by calculating the pressure−composition phase diagram. The coexistence of the single species solid and the fluid is determined by equating the chemical potential and pressure in fluid phase to those of the solid. For a binary compound in solid phase we use following condition to determine the coexistence with a fluid phase:

$$\frac{\mu_A^f + n\mu_B^f}{1+n} = G^s_{AB_n} \quad (17)$$

dx.doi.org/10.1021/jp5090907 | J. Phys. Chem. B XXXX, XXX, XXX−XXX

where μ^f are the chemical potential in the fluid phase and the $G^s_{AB_n}$ is the Gibbs energy per particle of the compound AB_n. In eq 17, the left-hand side refers to the chemical potential of a fluid when the species A and B are mixed to the composition of the solid, and the equation can be derived from the chemical equilibrium condition.[21] Figure 4 shows the pressure–composition phase diagram calculated at σ = 0.58 (solid line). The phase diagram predicted by simulation[18] is represented by the dashed line. Both AB_2 and AB_{13} structures appeared as stable structures, in agreement with the simulations[15,16,18,21] and experimental observations[24,25] overall in spite of some minor difference due to discrepancies in the free energies. At the size ratio of σ = 0.60 both AB_2 and AB_{13} appeared to be metastable. Bartlett et al. have also experimentally observed forming metastable[34] AB_{13} in a mixture of colloidal nanoparticles at size ratio of σ = 0.61 ± 0.02 and stable[24] AB_{13} at σ = 0.58. Moreover, we find the metastability of the AB (CsCl) structure at the size ratio of σ = 0.73 in agreement with the simulations.[15,18] Therefore, the FMT functional could be an efficient and reasonably accurate approach in determining the phase stability of complex binary systems.

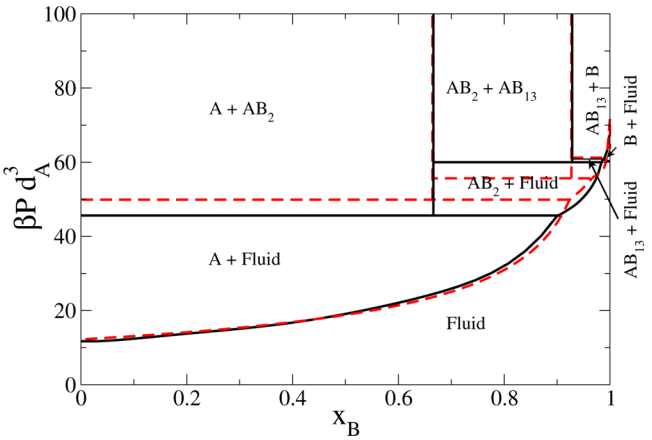

Figure 4. Pressure–composition phase diagram at σ = 0.58 for AB_{13} and AB_2 structures. The vertical axis is the pressure and the horizontal axis is the concentration of species B (x_B) in the fluid phase. The black solid lines represent the phase diagram calculated from FMT with the WB functional, and the dashed lines represent the simulation one.[18]

4. HARD SPHERE COMPLEXES IN THE Cu–Zr SYSTEM

Five hard sphere binary crystal structures appeared in the Cu–Zr system are studied. The simplest binary structure is the CuZr(B2)[29] (Figure 5d) which is also the AB structure studied in the previous section. The next structure near the 50% of Zr composition is the $CuZr_2(C11_b)$[30] structure (Figure 5e). This structure has six atoms in the unit cell. Each of the above-mentioned structures has two asymmetric sites corresponding to the Cu and the Zr atoms. The next crystal in this range is the $Cu_{10}Zr_7$-ϕ (prototype of $Ni_{10}Zr_7$), which belongs to the *Cmca* (64) space group[27,28] (Figure 5c). This structure has four asymmetric Zr sites and three Cu sites and has 68 atoms in a unit cell. In the Cu-rich side we studied two binary crystals. The $Cu_{51}Zr_{14}$(β) structure (Figure 5b) belongs to *P6/m*(175) space group and has 65 atoms in the unit cell. There are seven asymmetric Cu sites and three Zr sites. The fifth structure is the $Cu_5Zr(C15_b)$ structure (Figure 5a) in the *f*43*m* space group and has 24 atoms in the unit cell. It has five asymmetric sites of Cu atoms and one Zr site.

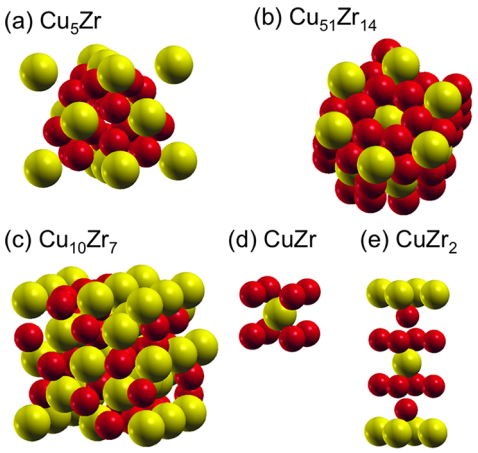

Figure 5. Sketch of the unit cells of the five binary crystals in the Cu–Zr system studied in this work. The red (dark) color represents Cu atoms, and yellow (light) color represents Zr atoms.

The most relevant quantity is to determine the hard sphere diameters consistently with all the structures in the system. We use an embedded atom model (EAM) potential describing the interactions in the Cu–Zr system.[35] In order to carry out perturbation calculations, we first convert the EAM potential to an effective pair potential ($\psi_{ab}(r_{ij})$) by performing a Taylor expansion of the embedding energy function around the host electron density of a given site (ρ^e_a).[36] Then we mapped the above crystal structures into two-component hard sphere systems whose interactions between the sites *a* and *b* are given by

$$\psi^{HS}_{ab}(r) = \begin{cases} +\infty, & r < d_{ab}(T) \\ 0, & r \geq d_{ab}(T) \end{cases} \tag{18}$$

The hard sphere diameter d_{ab} can be approximated to that of Barker and Henderson as

$$d_{ab} = \int_0^{\lambda_{ab}} (1 - e^{-\psi_{ab}(r)/k_B T})\, dr \tag{19}$$

It should be noted that the variation due to the asymmetric sites within a single species is averaged out, and all of the crystal structures are mapped to a two-component HS system. More details of this processes can be found in ref 37. The Zr atom has a larger diameter and is labeled as species A. Accordingly, it is found that the HS diameter ratio is around σ = 0.79. Small variations due to different crystal structures are also neglected, and all the five HS crystals are studied at σ = 0.79.

The FMT is employed to calculate the free energy of these model HS structures. The free energy functional in eq 4 is numerically integrated over a unit cell of each structures. Variational calculations with respect to two Gaussian parameters showed a clear global minimum in the solid region of the Gaussian parameter space for the structures of Cu_5Zr, $Cu_{51}Zr_{14}$, CuZr, and $CuZr_2$.

In Figure 6 the variation of the dimensionless Gaussian parameters ($\alpha_A d_A^2$ and $\alpha_B d_A^2$) as a function of η for the Cu_5Zr, $Cu_{51}Zr_{14}$, and $CuZr_2$ structures is shown. The α's corresponding to the global minimum of the Cu_5Zr structure first increases and then decreases when η > 0.60. This is similar to the previously reported behavior of the bcc lattice with the WB

dx.doi.org/10.1021/jp5090907 | J. Phys. Chem. B XXXX, XXX, XXX–XXX

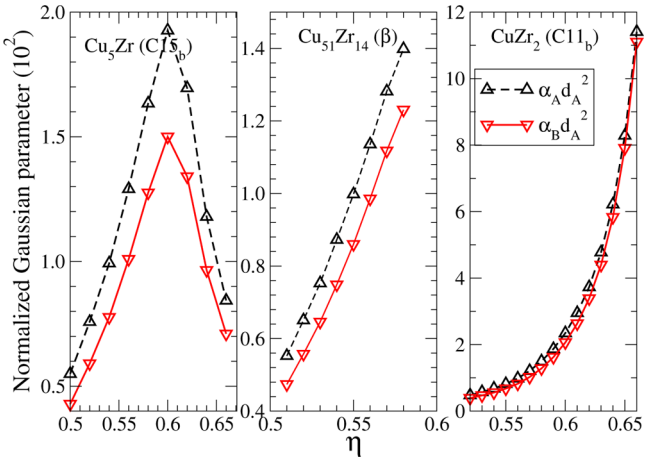

Figure 6. Normalized Gaussian parameter $\alpha_i d_A^2$ as a function of η for the model hard sphere crystals in the Cu−Zr system.

functional.[31] For the other structures, we observe that the α's are rapidly increasing as closing to the close packing limit.

The Lindemann ratio $L = \langle u^2 \rangle^{1/2}/R_0$, where $\langle u^2 \rangle$ is the mean square displacement and R_0 is the nearest-neighbor distance, is related to the Gaussian parameter as $L = [(2\alpha)^{1/2}R_0]^{-1}$. By assuming $R_0 \approx 1$ in dimensionless unit, the L of the lager species (Zr) of these binary crystals is calculated. In Figure 7 is

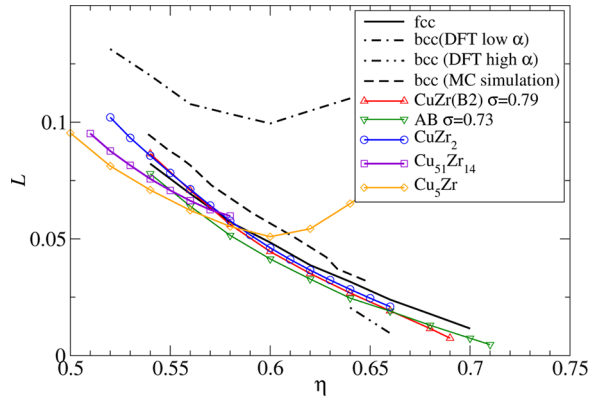

Figure 7. Lindemann ratio (L) as a function of η for the binary crystals in the Cu−Zr system (solid lines with symbols): $CuZr_2$, CuZr(B2) (at $\sigma = 0.73$ (AB) and $\sigma = 0.79$), $Cu_{51}Zr_{14}$, and Cu_5Zr. It should be noted that only the L of the larger species (Zr) is plotted and that of the smaller species also follows the same trend. The black solid line is for the single-component fcc lattice, and the dotted dash line is for the single-component bcc lattice obtained from the WB functionals. The dashed line is the L of bcc lattice calculated using Monte Carlo (MC) simulation data.[37]

plotted the variation of L against the η for these crystals. The L for the CuZr(B2) lattice is calculated at $\sigma = 0.79$ as well as $\sigma = 0.73$, which corresponds to the σ of the AB lattice studied in the section 3. The L of fcc (solid line) and bcc (dotted dash lines) lattices are also plotted for comparison. The dashed line is calculated for the single-component bcc lattice using the α from a recent Monte Carlo (MC) simulations.[37] This simulation results represent a physically acceptable solid phase for the bcc lattice. Generally, L of all the binary crystals are placed very close to that of fcc. The L of $CuZr_2$ and CuZr(B2) at both σ studied follow the fcc curve as approaching to the close packing limit. The approximate close packing fractions η of $CuZr_2$ and CuZr(B2) were estimated to be 0.71 and 0.705 at $\sigma = 0.79$, respectively. At $\sigma = 0.73$ the close packing limit is 0.72 for AB. Moreover as reaching the close packing limit L decreases toward zero, confirming the existence of stable solids in the two-dimensional Gaussian parameter space. The L of $Cu_{51}Zr_{14}$ also decreases as increasing η. In this case the close packing limit was observed at $\eta = 0.58$. Although the anomalous behavior of L is observed for the Cu_5Zr structure, it is well below the unphysical values of the bcc lattice (dotted dashed line in Figure 7). Thus, the observed global minimum in the Gaussian parameter space of these binary crystals would potentially represent a crystalline phase at low η.

The total free energy profile of these hard sphere crystals are plotted in Figure 8. The CuZr(B2) structure is a prototype of

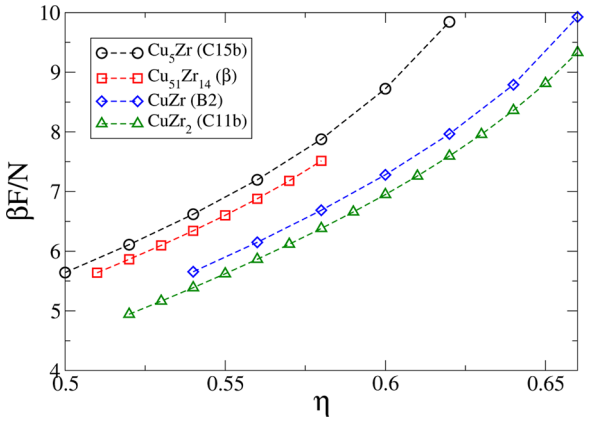

Figure 8. Total free energy as a function of η for the model hard sphere crystals in the Cu−Zr system.

the CsCl(AB). Here, the free energy of this structure is plotted at $\sigma = 0.79$. We observe the total free energy is increasing with η and overall reduction of the free energy as we move to the crystals with higher Zr composition. Thus, the WB functional seems to be able to provide a reasonable hard sphere reference system for the thermodynamics of alloys, which is used for the study of alloy phase diagrams.[38]

5. DISCUSSION

The latest development of the FMT, the WB functional, has several improvements over the previous versions. In particular, it has greatly improved the solid liquid coexistence conditions as a result of the accurate MCSL equation of state in the liquid phase.[3,11,14] It also has improved the free energy profile in the Gaussian parameter space.[3,31] The original Rosenfield version of the functional gave two minima for the fcc lattice. Except the true fcc minimum at higher α, the secondary minimum was observed in the range of $0.61 \leq \eta \leq 0.63$. Moreover when further increasing the density, a larger free energy barrier was developed between the liquid and the fcc solid region. The latest WB version of the functional seems to be free of these unphysical free energy profile. However, previous studies only focus on the region of $\eta < 0.70$. Our studies on the fcc at higher packing fractions ($\eta > 0.70$) show a similar behavior as the original Rosenfield version but now shifted to higher densities (see Figure 9). The onset of the secondary minimum (thick short arrow on Figure 9) was observed at $\eta \approx 0.716$ and developed into clear minimum as further increasing η. It is also observed the development of the energy barrier between the liquid and the true fcc minimum as the secondary minimum is

dx.doi.org/10.1021/jp5090907 | J. Phys. Chem. B XXXX, XXX, XXX−XXX

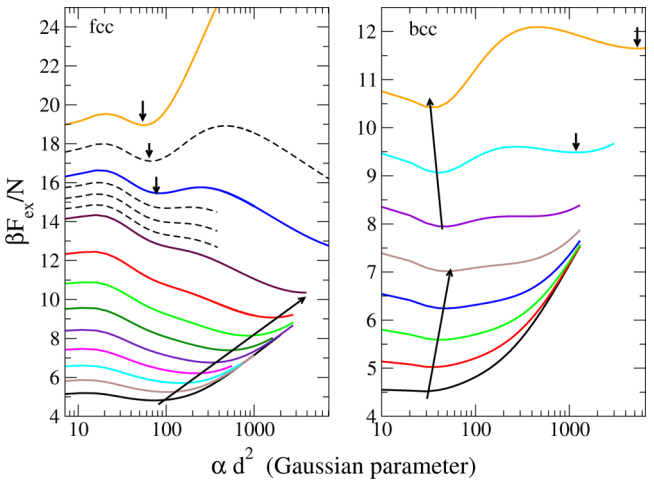

Figure 9. Exess free energy vs Gaussian parameter for the single-component fcc and bcc lattice calculated using the WB functional of FMT. For the fcc lattice the free energy landscape is calculated from η = 0.54−0.74 in steps of 0.02 (solid lines), and the dashed lines are at η = 0.704, 0.710, 0.716, and 0.73. For the bcc lattice the free energy is calculated at η = 0.52−0.66 in steps of 0.02 (solid lines). The long lines with arrows show the trend of the global minimum, and the short arrow headed lines show the secondary minimum observed.

further developed. In this case the true fcc minimum (the trend is shown by the long arrows) is the global minimum and the secondary minimum gives a metastable solid phase. Using the WBII functional,[39,40] similar results are also observed.[41]

The single-component bcc lattice also has the problem of double minima.[31,42] In this case the global minimum (lower α) is not the true thermodynamic stable phase.[31] However, when the bcc lattice is distorted into AB-like structure by changing the diameter of a basis atom, a unique minimum in the two-dimensional Gaussian parameter space is observed. The minimum search in 2D was done numerically. The search started from $\alpha_i d_A^2 \approx 100$, and the minimum was observed at $\alpha_A d_A^2$ = 22 958 and $\alpha_B d_A^2$ = 12 780 for σ = 0.73 and η = 0.71. We did not see any noticeable secondary minimum developed in this wide minimization path. The maximum packing fraction at σ = 0.73 is $\eta \approx 0.72$, and that of σ = 0.79 is $\eta \approx 0.705$. In comparing with the simulations (Figure 2), excess free energy shows a reasonably good agreement with simulations. Furthermore, using the HS free energies and the Gaussian parameters, we performed perturbation calculations for the binary metallic crystals in the Cu−Zr system. It is observed that the Helmholtz free energies of these crystals show very good agreement with the simulation data.[38] Thus, we can clearly state that the minima observed from WB functional (both free energies and α's) for the HS model crystals of the Cu−Zr system have true physical meaning.

However, the $Cu_{10}Zr_7$ structure does not show a minimum in the two-dimensional Gaussian parameter space. The free energy minimum is observed in the liquid limit where α_A, $\alpha_B \rightarrow 0.0$ and rapidly diverges as going away from zero in the two-dimensional Gaussian parameter space. Similar unphysical behavior on the single-component simple cubic (sc) lattice has also been observed recently.[31] Some discrepancies may arise due to the Gaussian parametrization (isotropic) of the density profile. Recent work has focused on the free minimization of the FMT functional with anisotropic density distributions.[42−44] However, a similar anomaly in the bcc hard sphere crystal has been reported.[42] Therefore, we attribute the failure of the $Cu_{10}Zr_7$ structure to some artifact of of this FMT functional.

6. CONCLUSIONS

Using the fundamental measure density functional, we calculate the free energies of binary hard sphere crystals. Our results of three stable hard sphere crystals (AB, AB_2, and AB_{13}) which has been previously studied using simulations and experiments demonstrate the reliability of the FMT for complex hard sphere crystal structures. The calculated free energy and pressure yield a reasonable agreement with the simulation results and reproduce the correct phase stability observed in simulations and experiments. Five hard sphere model structures existing in the Cu−Zr system are also studied using the FMT. Four of them yield stable solids in the two-dimensional Gaussian parameter space which can be used as a reference system for perturbation calculations. However, the $Cu_{10}Zr_7$ structure does not show a clear minimum in the Gaussian parameter space representing a solid phase. This instability could have similar origin as the previously reported bcc lattice of the hard sphere system and fcc lattice in higher densities observed in this study.

Even though the current version of FMT cannot provide a HS reference system for all of the crystalline phases (such as sc or $Cu_{10}Zr_7$) due to the thermodynamic instability of the current functional, it does provide a reliable and efficient reference system for most of the crystalline structures as shown in this study. In combination with the single occupancy Monte Carlo method[45] the hard sphere reference system using FMT can provide an efficient way to estimate the entropic contribution to the free energy of real systems as demonstrated in this report and a recent report for the bcc case.[37]

AUTHOR INFORMATION

Corresponding Author

*E-mail: xsong@iastate.edu (X.S.).

Notes

The authors declare no competing financial interest.

ACKNOWLEDGMENTS

We are grateful to an anonymous referee for including the data of fcc crystal from the WBII functional that agree with the observation that there exists a secondary minimum at low alpha with high packing fractions (Figure 9). This research was sponsored by the Division of Materials Sciences and Engineering, Office of Basic Energy Sciences, U.S. Department of Energy, under Contract W-7405-ENG-82 with Iowa State University.

REFERENCES

(1) Evans, R. Nature of the Liquid-Vapor Interface and Other Topics in the Statistical-Mechanics of Nonuniform, Classical Fluids. *Adv. Phys.* **1979**, *28*, 143−200.

(2) Hansen, J. P.; McDonald, I. R. *Theory of Simple Liquids*; Academic: London, 1986.

(3) Roth, R.; Evans, R.; Lang, A.; Kahl, G. Fundamental Measure Theory for Hard-Sphere Mixtures Revisited: The White Bear Version. *J. Phys.: Condens. Matter* **2002**, *14*, 12063.

(4) Tarazona, P. Density Functional for Hard Sphere Crystals: A Fundamental Measure Approach. *Phys. Rev. Lett.* **2000**, *84*, 694−697.

(5) Warshavsky, V. B.; Song, X. Fundamental Measure Density Functional Theory Studies on the Freezing of Binary Hard-Sphere and Lennard-Jones Mixtures. *J. Chem. Phys.* **2008**, *129*, 034506.

(6) Song, X.; Morris, J. R. Accurate Method to Calculate Liquid and Solid Free Energies for Embedded Atom Potentials. *Phys. Rev. B* **2003**, *67*, 092203.
(7) Warshavsky, V. B.; Song, X. Phase Diagrams of Binary Alloys Calculated from a Density Functional Theory. *Phys. Rev. B* **2009**, *79*, 014101.
(8) Rosenfeld, Y. Free-Energy Model for the Inhomogeneous Hard-Sphere Fluid Mixture and Density-Functional Theory of Freezing. *Phys. Rev. Lett.* **1989**, *63*, 980−983.
(9) Rosenfeld, Y. Free-Energy Model for the Inhomogeneous Hard-Sphere Fluid: "Closure" Relation Between Generating Functionals for "Direct" and "Cavity" Distribution Functions. *J. Chem. Phys.* **1990**, *93*, 4305−4311.
(10) Roth, R.; Dietrich, S. Binary Hard-Sphere Fluids Near a Hard Wall. *Phys. Rev. E* **2000**, *62*, 6926−6936.
(11) Tarazona, P. Fundamental Measure Theory and Dimensional Interpolation for the Hard Spheres Fluid. *Physica A* **2002**, *306*, 243−250.
(12) Warshavsky, V. B.; Song, X. Fundamental-Measure Density Functional Theory Study of the Crystal-Melt Interface of the Hard Sphere System. *Phys. Rev. E* **2006**, *73*, 031110/1−031110/6.
(13) Rosenfeld, Y.; Schmidt, M.; Löwen, H.; Tarazona, P. Fundamental-Measure Free-Energy Density Functional for Hard Spheres: Dimensional Crossover and Freezing. *Phys. Rev. E* **1997**, *55*, 4245−4263.
(14) Yu, Y.-X.; Wu, J.; Xin, Y.-X.; Gao, G.-H. Structures and Correlation Functions of Multicomponent and Polydisperse Hard-Sphere Mixtures from a Density Functional Theory. *J. Chem. Phys.* **2004**, *121*, 1535−1541.
(15) Eldridge, M.; Madden, P.; Frenkel, D. The Stability of the AB_{13} Crystal in a Binary Hard Sphere System. *Mol. Phys.* **1993**, *79*, 105−120.
(16) Eldridge, M.; Madden, P.; Frenkel, D. A Computer Simulation Investigation into the Stability of the AB_2 Superlattice in a Binary Hard Sphere System. *Mol. Phys.* **1993**, *80*, 987−995.
(17) Eldridge, M.; Madden, P.; Frenkel, D. Entropy-Driven Formation of a Superlattice in a Hard-Sphere Binary Mixture. *Nature* **1993**, *365*, 35−37.
(18) Jackson, A. N.; Ackland, G. J. Lattice-Switch Monte Carlo Simulation for Binary Hard-Sphere Crystals. *Phys. Rev. E* **2007**, *76*, 066703.
(19) Xu, H.; Baus, M. A Density Functional Study of Superlattice Formation in Binary Hard-Sphere Mixtures. *J. Phys.: Condens. Matter* **1992**, *4*, L663.
(20) Smithline, S. J.; Haymet, A. D. J. Density Functional Theory for the Freezing of 1:1 Hard Sphere Mixtures. *J. Chem. Phys.* **1987**, *86*, 6486−6494.
(21) Cottin, X.; Monson, P. A. Substitutionally Ordered Solid Solutions of Hard Spheres. I. *Chem. Phys.* **1995**, *102*, 3354−3360.
(22) Sanders, J. V. Close-Packed Structures of Spheres of Two Different Sizes I. Observations on Natural Opal. *Philos. Mag. A* **1980**, *42*, 705−720.
(23) Yoshimura, S.; Hachisu, S.; Nakagaski, M.; Shinoda, K.; Matijevi, E. Frontiers in Colloid Science In Memoriam Professor Dr. Bun-ichi Tamamushi. *Prog. Colloid Polym. Sci.* **1983**, *68*, 59−70.
(24) Bartlett, P.; Ottewill, R. H.; Pusey, P. N. Superlattice Formation in Binary Mixtures of Hard-Sphere Colloids. *Phys. Rev. Lett.* **1992**, *68*, 3801−3804.
(25) Frenkel, D. Entropy-Driven Formation of a Superlattice in a Hard-Sphere Binary Mixture. *Nat. Mater.* **2006**, *5*, 85−86.
(26) Gabathuler, J.-P.; White, P.; Parth, E. $Zr_{14}Cu_{51}$ and $Hf_{14}Cu_{51}$ with $GdAg_{3.6}$ Structure Type. *Acta Crystallogr., Sect. B* **1975**, *31*, 608−610.
(27) Glimois, J.; Forey, P.; Feron, J.; Becle, C. Structural Investigations of the Pseudo-Binary Compounds $Ni_{10-x}Cu_xZr_7$. *J. Less-Common Met.* **1981**, *78*, 45−50.
(28) Albisetti, A. F.; Biffi, C.; Tuissi, A. Synthesis and Structural Analysis of $Cu_{10}Zr_7$. *J. Alloys Compd.* **2012**, *544*, 42−45.
(29) Carvalho, E.; Harris, I. Constitutional and Structural Studies of the Intermetallic Phase, ZrCu. *J. Mater. Sci.* **1980**, *15*, 1224−1230.
(30) Nevitt, M. V.; Downey, J. A. Family of Intermediate Phases Having the Si_2 Mo-Type Structure. *Trans. TMS-AIME* **1962**, *224*, 195.
(31) Lutsko, J. F. Properties of Non-Fcc Hard-Sphere Solids Predicted by Density Functional Theory. *Phys. Rev. E* **2006**, *74*, 021121.
(32) Mermin, N. D. Thermal Properties of the Inhomogeneous Electron Gas. *Phys. Rev.* **1965**, *137*, A1441−A1443.
(33) Mansoori, G. A.; Carnahan, N. F.; Starling, K. E.; Leland, T. W. Equilibrium Thermodynamic Properties of the Mixture of Hard Spheres. *J. Chem. Phys.* **1971**, *54*, 1523−1525.
(34) Bartlett, P.; Ottewill, R. H.; Pusey, P. N. Freezing of Binary Mixtures of Colloidal Hard Spheres. *J. Chem. Phys.* **1990**, *93*, 1299−1312.
(35) Mendelev, M.; Kramer, M.; Ott, R.; Sordelet, D.; Yagodin, D.; Popel, P. Development of Suitable Interatomic Potentials for Simulation of Liquid and Amorphous CuZr Alloys. *Philos. Mag.* **2009**, *89*, 967−987.
(36) Foiles, S. M. Application of the Embedded-Atom Method to Liquid Transition Metals. *Phys. Rev. B* **1985**, *32*, 3409−3415.
(37) Warshavsky, V. B.; Song, X. Perturbation Theory of Solid-Liquid Interfacial Free Energies of Bcc Metals. *Phys. Rev. E* **2012**, *86*, 031602.
(38) Gunawardana, K. G. S. H.; Wilson, S. R.; Mendelev, M. I.; Song, X. Theoretical Calculation of the Melting Curve of Cu-Zr Binary Alloys. *Phys. Rev. E* **2014**, *90*, 052403.
(39) Hansen-Goos, H.; Roth, R. Density Functional Theory for Hard-Sphere Mixtures: The White Bear Version Mark II. *J. Phys.: Condens. Matter* **2006**, *18*, 8413−8425.
(40) Oettel, M.; Gorig, S.; Hartel, A.; Lowen, H.; Radu, M.; Schilling, T. Free Energies, Vacancy Concentrations, and Density Distribution Anisotropies in Hard-Sphere Crystals: A Combined Density Functional and Simulation Study. *Phys. Rev. E* **2010**, *82*, 051404.
(41) An anonymous referee sent us the free energy data as a function of α for FCC using the WBII functional.
(42) Yamani, M. H.; Oettel, M. Stable and Metastable Hard-Sphere Crystals in Fundamental Measure Theory. *Phys. Rev. E* **2013**, *88*, 022301.
(43) Oettel, M.; Görig, S.; Härtel, A.; Löwen, H.; Radu, M.; Schilling, T. Free Energies, Vacancy Concentrations, and Density Distribution Anisotropies in Hard-Sphere Crystals: A Combined Density Functional and Simulation Study. *Phys. Rev. E* **2010**, *82*, 051404.
(44) Härtel, A.; Oettel, M.; Rozas, R. E.; Egelhaaf, S. U.; Horbach, J.; Löwen, H. Tension and Stiffness of the Hard Sphere Crystal-Fluid Interface. *Phys. Rev. Lett.* **2012**, *108*, 226101.
(45) Hoover, W. G.; Ree, F. H. Melting Transition and Communal Entropy for Hard Spheres. *J. Chem. Phys.* **1968**, *49*, 3609.

dx.doi.org/10.1021/jp5090907 | *J. Phys. Chem. B* XXXX, XXX, XXX−XXX